Results in Physics 16 (2020) 103022

Contents lists available at ScienceDirect

Results in Physics

journal homepage: www.elsevier.com/locate/rinp

Highly sensitive photonic crystal fiber salinity sensor based on Sagnac interferometer

Md. Aslam Mollah[a,*,1], Md. Yousufali[a], Md. Rifat Bin Asif Faysal[a], Md. Rabiul Hasan[b], Md. Biplob Hossain[c], I.S. Amiri[d,e,*,1]

[a] Department of Electronics & Telecommunication Engineering, Rajshahi University of Engineering & Technology, Rajshahi 6204, Bangladesh
[b] Department of Physics and Technology, University of Tromso, 9037 Tromso, Norway
[c] Department of Electrical and Electronic Engineering, Jashore University of Science and Technology, Jashore 7408, Bangladesh
[d] Computational Optics Research Group, Advanced Institute of Materials Science, Ton Duc Thang University, Ho Chi Minh City, Viet Nam
[e] Faculty of Applied Sciences, Ton Duc Thang University, Ho Chi Minh City, Viet Nam

ARTICLE INFO

Keywords:
Finite element method
Photonic crystal fiber
Sea water
Sensor

ABSTRACT

For a sensor, high sensitivity, structural simplicity, and longevity are highly desired for measurement of salinity in seawater. This work proposed an ultrahigh sensitive photonic crystal fiber (PCF) salinity sensor based on the sagnac interferometer (SI). The propagation characteristics of the proposed PCF are analyzed by the finite element method (FEM). The achieved sensitivity reaches up to 37,500 nm/RIU and 7.5 nm/% in the salinity range from 0% to 100%. The maximum resolutions of 2.66×10^{-06} RIU and 1.33×10^{-02}% are achieved with high linearity of 0.9924 for 2.20 cm length of the proposed PCF. Owing to such excellent results, this proposed sensor offers the potential to measure the salinity of seawater.

Introduction

Measurement of salt level in seawater is essential as it has significant effect on seawater organism and submarine activities. Mainly, salinity is measured based on the electrical conductivity of chloride ions. However, this measurement process is affected by the interferences from other contaminant ions [1]. In this regard, fiber optic salinity sensors have arisen interest to the researchers because of several advantages like electromagnetic interference (EMI) immunity, compactness, remote sensing, tunable dispersion and controllable birefringence [2].

To date, several optical fiber salinity sensors have been proposed to achieve high sensitivity and structural simplicity. For instance, a hydrogel coated fiber Bragg grating (FBG) salinity sensor was fabricated by *J. Cong et al.* [3]. Soon later, *X. Liu et al.* [4] optimized the same structure by etching the cladding and achieved sensitivity about 10.4 pm/%. Very recently, *M. Sun et al.* [5] proposed an experimental study of FBG based salinity sensor and achieved sensitivity of −0.0358 nm/%. Though FBG sensors have simple structure and are suitable for long-term measurement process, they exhibits very low sensitivity. *D. J. Gentleman et al.* demonstrated a surface plasmon resonance (SPR) based metal coted optical fiber salinity sensor having sensitivity of 200 pm/% [6]. In SPR phenomena, electromagnetic waves are coupled with free electron oscillations at the metal-dielectric interface under *p*-polarized light radiation [7]. The sensing properties of SPR sensors depend on the metallic materials. Among the various types of plasmonic materials, gold and silver are the most common ones due to their relatively low loss in the visible and near-infrared region [8]. Although SPR based salinity sensors have comparatively high sensitivity, fabrication of SPR sensors is challenging as they require metal film deposition. Besides that, due to the metal film, these sensor are not suitable for long-term measurement process as the seawater is strong corrosive. Sensor based on microfiber knot resonator [9], and nanocavity photonic crystal resonator [10] are demonstrated for the purpose of salinity concentration measurement of sea water but the reported sensitivities are very low of 21.18 pm/% and 544 nm/RIU, respectively. Moreover, sensor based on two-core fiber [11,12], tapered fiber [13], U-shaped fiber [14], long period grating (LPG) [15] have been also proposed. But these sensors also have low sensitivity. Furthermore, many work for simultaneous sensing of salinity and temperature have been done [16–21], but the outcomes are not so promising. In recent days, Sagnac interferometer (SI) based sensors are widely used in

* Corresponding authors at: Rajshahi University of Engineering & Technology, Rajshahi 6204, Bangladesh (Md. Aslam Mollah); Ton Duc Thang University, Ho Chi Minh City, Viet Nam (I.S. Amiri).
E-mail addresses: ruet10aslam@gmail.com (Md. Aslam Mollah), biplobh.eee10@gmail.com (Md. B. Hossain), irajsadeghamiri@tdtu.edu.vn (I.S. Amiri).
[1] These authors contributed equally to this work and co-corresponding authors.

https://doi.org/10.1016/j.rinp.2020.103022
Received 25 January 2020; Received in revised form 18 February 2020; Accepted 19 February 2020
Available online 20 February 2020

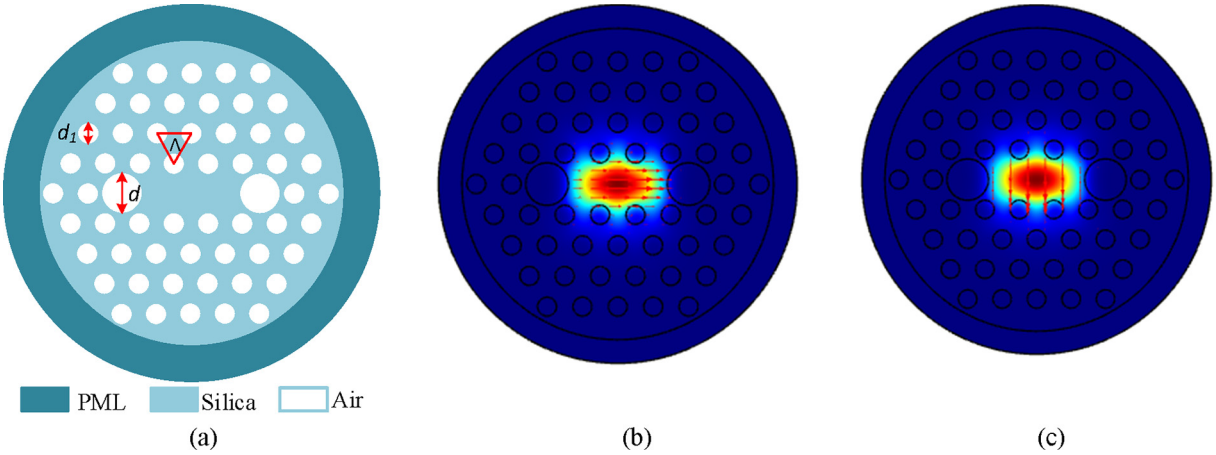

Fig. 1. The proposed seawater filled PCF with $\Lambda = 3$ μm, $d = 1.6$ μm, $d_1 = 3.6$ μm, and $PML = 2$ μm (a) Cross-section view (b) Field distribution in x-pol.(c) Field distribution in y-pol.

sensing application such as temperature [22], pressure [23], magnetic field [24] and glucose sensor [25] due to its compactness, high sensitivity, and easy fabrication. Besides that, SI sensors are suitable for long hours work under seawater [1].

In this paper, a simple photonic crystal fiber (PCF) salinity sensor based on SI is presented. The guiding characteristics are investigated using finite element method (FEM) based COMSOL software with optimized thingness of perfect match layer (PML). All the air holes of the four rings hexagonal lattice PCF are proposed to be filled by the sea water. Two big air holes create large birefringence in the proposed structure that significantly helps to achieve high sensitivity. Moreover, the optimum length of the proposed sensor is chosen based on the sensitivity and the linearity response.

Sensor design and theoretical modelling

The cross section of the proposed salinity sensor is illustrated in Fig. 1(a) and field distribution of *x*- and *y*-polarization is shown in Fig. 1(b) and (c), respectively. All the air holes are organized in triangular lattice, where the two adjacent air holes distance is Λ. Three air holes from the center are eliminated, that forms the core of the PCF. Two air holes having diameter d along the horizontal axis are kept large from the regular air hole diameter d_1, which creates asymmetry in the fiber structure. As a result, the fiber birefringence increases. The material dispersion of the fiber material (fused silica) is calculated by the Sellmeier formula [1].

$$n(\lambda) - 1 = \sum_{k=1}^{3} \frac{X_k \lambda^2}{\lambda^2 - Y_k} \tag{1}$$

where $n(\lambda)$ is the refractive index of silica at wavelength λ (μm) and X_k and Y_k are the constants. The value of the constant X_1, X_2, X_3, Y_1, Y_2, and Y_3 are 69.6163×10^{-2}, 40.79426×10^{-2}, 89.74794×10^{-2}, 46.914826×10^{-4}, $13.5120631 \times 10^{-3}$, and 97.9340025, respectively. All air holes are proposed to be filled by the sea water whose refractive index (RI) can be expressed as follows [2],

$$\begin{aligned} n_{sw} &= 1.31405 + (1.779 \times 10^{-4} - 1.05 \times 10^{-6} + 1.6 \times 10^{-8} T^2)S - 2.02 \\ &\times 10^{-6} T^2 + (15.868 + 0.1155S - 4.23 \times 10^{--3} T)/\lambda - 4380/\lambda^2 + \\ &1.1455 \times 10^6/\lambda^3 \end{aligned} \tag{2}$$

where, T, S, and λ indicates room temperature (°C), salinity (%), and wavelength (μm), respectively. Solution having same salinity may have different refractive index due to other components (MgCL2, MgSO4) which may create cross-sensitivity problem. However, NaCl is the main component of inorganic salts (several orders of magnitude larger than other salts) in seawater [1]. Hence, the probability of cross sensitivity is very low.

Liquid infiltration is quite popular in different sensing application such as temperature [22], glucose [25], salinity [2], and magnetic field [26]. With regard to liquid infiltration into the fiber air holes, many techniques have been proposed theoretically and experimentally. Liquid filling process into the PCF air holes by the FBG fiber with collapsed cladding holes is demonstrated by *K. Nielsen et al.* [27]. Technique assisted by focused ion beam and femtosecond laser are also proposed by *F. Wang et al* [28] and *Y. Wang et al.* [29], respectively. Using these techniques, even an air hole having diameter of 1 μm is possible to fill up by the fluid. The minimum air hole diameter of the proposed PCF is 1.6 μm. So we presumed that the sea water can be infiltrated in to the PCF by pumping or any of these existing techniques.

A typical setup for measuring salinity using SI is shown in Fig. 2. A broadband source (BBS) generates a beam of light which is divided into two beams after encountered at the 3 dB coupler. Then these two beams, one in clockwise and the other in anticlockwise, travel through the sea water filled PCF. Finally, the two beams couple when they meet at the 3 dB coupler again. The polarization controller (PC) can be used

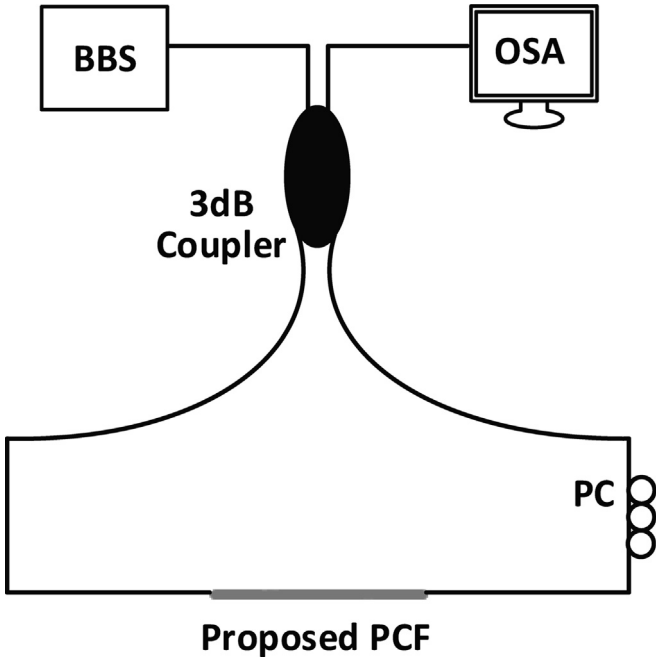

Fig. 2. Sagnac interferometer generalized setup.

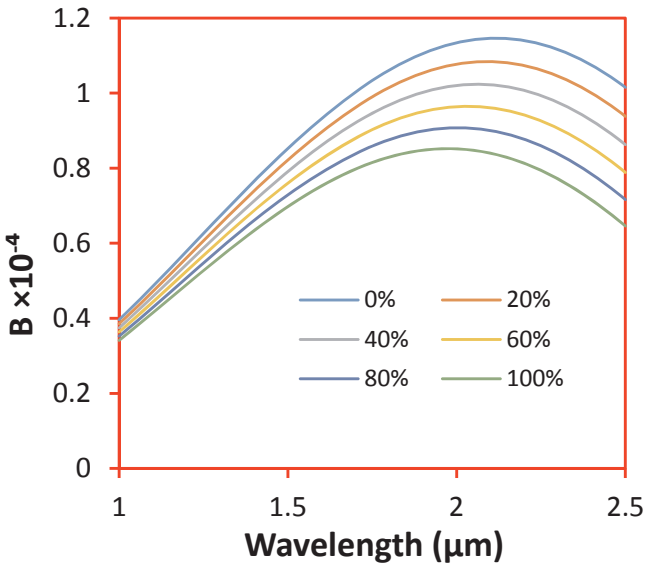

Fig. 3. Birefringence (B) variation with salinity.

to adjust the polarization state of the light. The two beams have phase difference due to birefringence of the designed PCF. Besides that, according to the Eq. (2), with the variation of the salinity, the RI of the water varies that changes the birefringence too. Thus, the interference spectrum changes with the variation of the salinity which can be observed in the optical spectrum analyser (OSA).

The normalized power at 3 dB coupler can be obtained by the following equation [22],

$$P(\text{dB}) = [1 - \cos(2\pi BL/\lambda)]/2 \tag{3}$$

where, $2\pi BL/\lambda$ denotes the phase difference and B indicates the birefringence which is equal to $|n_j - n_k|$, n_j and n_k are the effective RI in x- and y-polarization, respectively. L denotes the length of the proposed PCF. When BL/λ is an integer then the phase matching condition is satisfied. As a result, a dip is found at the interference spectrum.

Results and discussion

The birefringence (B) of the proposed PCF as a function of wavelength by varying the salinity lavel is illustrated in Fig. 3. As all the air holes are filled by the sea water, different salinity level of the water can directly vary the distribution of RI of the PCF and then leads to the variation in the birefringence. From Fig. 3, it can be noticed that at the same salinity level, with the increasing of the wavelength the birefringence increases and then decreases. On the other hand, the birefringence decreases with the increasing of the salinity level as the index difference between silica and sea water is decreased with the increasing of salinity.

The interference spectrum with fiber length 2.15, 2.20, 2.25, and 2.30 cm are shown in Fig. 4(a)–(d), respectively. In those figures, two dips are found, the dip 1 covers wavelength from 1000 nm to 1500 nm and the dip 2 covers wavelength from 1700 nm to 2500 nm. It can be noticed that dip 1 experiences a red shift while dip 2 experiences an

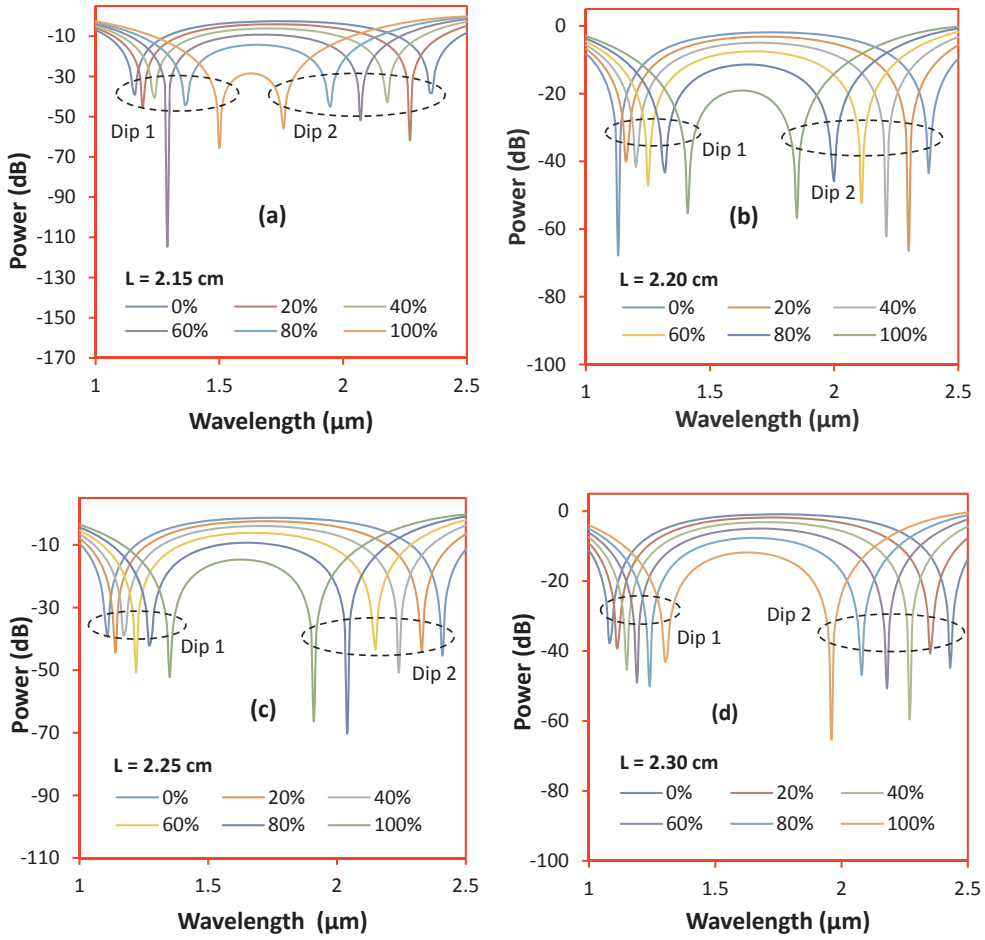

Fig. 4. Normalized power spectrum of the proposed sea water filled PCF with the variation of salinity in sea water for (a) 2.15 cm, (b) 2.20 cm, (c) 2.25 cm and (d) 2.30 cm sensor length.

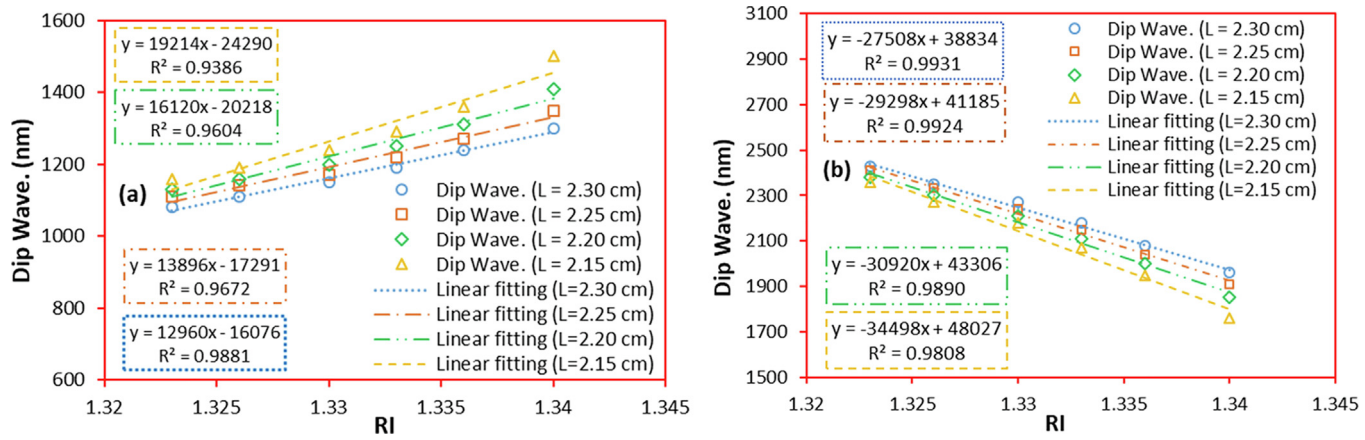

Fig. 5. Linear fitting of dip wavelength for (a) dip 1 and (b) dip 2 with the variation of salinity in the sea water for different sensor length.

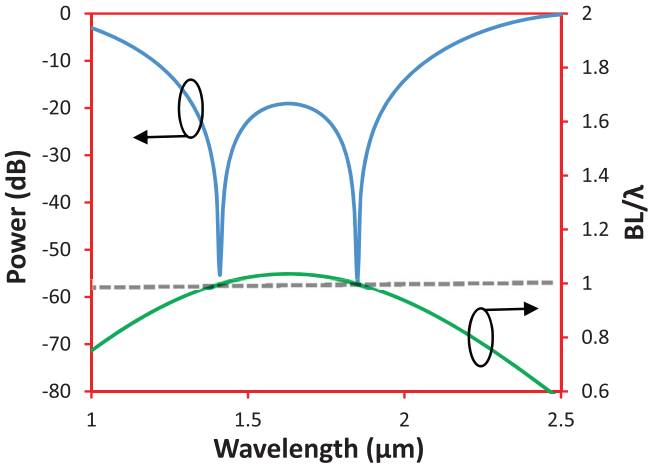

Fig. 6. Normalized power spectrum and BL/λ as a function of wavelength at 100% salinity for L = 2.20 cm.

obvious blue shift. This is because with the variation of wavelength the birefringence increase first and then decrease as illustrated in Fig. 3 [25]. It can be also seen that dip 2 experiences greater shift than dip 1. That mainly because that the birefringence difference between two successive salinity level is insignificance in shorter wavelength (dip 1) and it is high in the higher wavelength (dip 2). Therefore, the proposed sensor offers higher sensitivity at dip 2 than that of dip 1. Although the sensitivity at dip 1 is comparatively lower, dip 1 offers low cost sensing as the light sources are commercially available in shorter wavelength region. Hence, both dip 1 and dip 2 are taken in to consideration for sensitivity analysis. The dip wavelength (DW) variation due to the change of salinity for dip 1 and dip 2 is shown in Fig. 5(a) and (b), respectively. According to the linear fitting characteristics, the proposed salinity sensor exhibits average sensitivity of 19,214 nm/RIU, 16,120 nm/RIU, 13,896 nm/RIU and 12,960 nm/RIU for fiber length of 2.15 cm, 2.20 cm, 2.25 cm, and 2.30 cm, respectively, for dip 1. On the other hand, for dip 2, the average sensitivities are 34,498 nm/RIU, 30,920 nm/RIU, 29,298 nm/RIU and 27,508 nm/RIU for fiber length of 2.15 cm, 2.20 cm, 2.25 cm, and 2.30 cm, respectively. As mention earlier, dips are found only when the value of BL/λ is equal to an integer [22] as illustrated in Fig. 6. From Fig. 6 it can be seen that dips are found only when the value of BL/λ is equal to 1. Hence, dip wavelength is directly dependent on the birefringence. As the change of birefringence (B) with the wavelength (λ) of our proposed sensor is not linear in the entire operating range (also the birefringence is different at different wavelength), wavelength shift with the variation of length is also nonlinear. However, it is found that sensitivity can be increased by decreasing the sensor length but at the cost of linearity. Therefore, the sensor length is selected to 2.20 cm as a trade-off between sensitivity and linearity.

The sensitivity and resolution of the sensor at different salinity level can be calculated using Eqs. (4) [30,31] and (5) [2], respectively.

$$s_w = \frac{\partial\lambda}{\partial n_{sw}}(nm/\mathrm{RIU}) = \frac{\partial\lambda}{\partial S}(nm/\%) \tag{4}$$

$$s_R = \partial n_{sw} \times \frac{\lambda_{\min}}{\partial\lambda}(\mathrm{RIU}) = \partial S \times \frac{\lambda_{\min}}{\partial\lambda}(\%) \tag{5}$$

where $\partial\lambda$ is the shift of DW due to change of salinity (∂S) in the sea water or change of RI of sea water (∂n_{sw}). For the optimum sensor length of L = 2.20 cm, the blue shift of DW from 1.13 μm to 1.16 μm is found by varying the salinity from 0% to 20% at dip 2. Therefore, according to the Eq. (4), the sensitivity of 7500 nm/RIU and 1.5 nm/% are calculated at 20% salinity. Considering OSA resolution (λ_{min}) of

Table 1
Proposed salinity sensor's performance at different salinity.

Salt (%)	∂n_{sw} (RIU)	∂S (%)	Dip	Dip Wave. (nm)	$\partial\lambda$ (nm)	Sw (nm/RIU)	Sw (nm/%)	S_R (RIU)	S_R (%)
0	N/A	N/A	dip 1	1130	N/A	N/A	N/A	N/A	N/A
			dip 2	2380	N/A	N/A	N/A	N/A	N/A
20	0.004	20	dip 1	1160	30	7500	1.5	1.33×10^{-05}	6.67×10^{-02}
			dip 2	2300	80	20,000	4.0	5.00×10^{-06}	2.50×10^{-02}
40	0.003	20	dip 1	1200	40	13,333	2.0	7.50×10^{-06}	5.00×10^{-02}
			dip 2	2210	90	30,000	4.5	3.33×10^{-06}	2.22×10^{-02}
60	0.004	20	dip 1	1250	50	12,500	2.5	8.00×10^{-06}	4.00×10^{-02}
			dip 2	2110	100	25,000	5.0	4.00×10^{-06}	2.00×10^{-02}
80	0.003	20	dip 1	1310	60	20,000	3.0	5.00×10^{-06}	3.33×10^{-02}
			dip 2	2000	110	36,666.67	5.5	2.72×10^{-06}	1.82×10^{-02}
100	0.004	20	dip 1	1410	100	25,000	5.0	4.00×10^{-06}	2.00×10^{-02}
			dip 2	1850	150	37,500	7.5	2.66×10^{-06}	1.33×10^{-02}

Table 2
Sensitivity comparison among different salinity sensor.

Ref.	Max. Sensitivity	Max. Resolution
PCF sensor [2]	5675 nm/RIU	—
Hydrogel coated FBG sensor [4]	10.4 pm/%.	—
Lamellar polyimide coated FBG sensor [5]	−0.0358 nm/%	—
Au-Cr Coated SPR sensor [6]	200 pm/%	—
Microfiber knot resonator [9]	21.18 pm/%	—
Nano-cavity photonic crystal resonator [10]	544 nm/RIU	—
Two core fiber sensor [11]	1400 nm/RIU	—
Tapered fiber sensor [12]	2834.3 nm/RIU	—
U-shaped fiber sensor [14]	—	1×10^{-03}
LPG sensor [15]	−39.1 nm/RIU	—
Tri-core PCF sensor [16]	5674 nm/RIU	—
D-shaped sensor [17]	1.6 nm/%	—
Fabry-Perot interferometer sensor [18]	6830 nm/RIU	—
Microfiber directional coupler sensor [19]	930 pm/%	—
Polydimethylsiloxane coated SPR sensor [20]	0.0558 nm/%	—
C-Type fiber sensor [20]	1.402 nm/%	—
Proposed work	37,500 nm/RIU and 7.5 nm/%	2.66×10^{-06} RIU and 1.33×10^{-02}%

0.1 nm, corresponding sensor resolution (R) is calculated of 1.33×10^{-06} RIU and 6.67×10^{-02}% by using Eq. (5). The sensitivity of the designed sensor for different salt level is noted at Table 1. The maximum sensitivity of the proposed salinity sensor reaches up to 37,500 nm/RIU and 7.5 nm/% at 100% salinity for dip 2.

A number of previously reported salinity sensors with their corresponding sensitivity is summarized at Table 2. According to the Table 2, our proposed sea water filled PCF exhibits few times better sensitivity than other sensors reported in the literature. At the same time, the proposed PCF has very simple and common structure. So we believe that our PCF will be easy to fabricate.

Conclusion

A PCF salinity sensor based on SI is numerically investigated in this paper. All the air holes of the PCF are proposed to be filled by the different salinity concentration of sea water. Two air holes along the horizontal axis are intentionally kept large to introduce birefringence in the fiber structure. However, with the variation of the salinity, the RI of the sea water changes that leads to the change in the fiber birefringence. Hence, a shift of dip wavelength is observed with the variation of the salinity. By observing these wavelength shift, it is found that the designed sensor's sensitivity reaches up to 37,500 nm/RIU and 7.5 nm/% in the salinity range from 0% to 100%. Besides that, the average sensitivity of the sensor is also high as 29,298 nm/RIU. Owing to such promising results and simple structure, the proposed sensor has immense potential for salinity measurement of seawater.

Declaration of Competing Interest

The authors declare that they have no known competing financial interests or personal relationships that could have appeared to influence the work reported in this paper.

Appendix A. Supplementary data

Supplementary data to this article can be found online at https://doi.org/10.1016/j.rinp.2020.103022.

References

[1] Qian Y, Zhao Y, Wu Ql, Yang Y. Review of salinity measurement technology based on optical fiber sensor. Sens Actuators, B 2018;260:86–105.
[2] Vigneswaran D, Ayyanar N, Sharma M, Sumathi M, Rajan M, Porsezian K. Salinity sensor using photonic crystal fiber. Sens Actuators, A 2018;269:22–8.
[3] Cong J, Zhang X, Chen K, Xu J. Fiber optic Bragg grating sensor based on hydrogels for measuring salinity. Sens Actuators, B 2002;87:487–90.
[4] Liu X, Zhang X, Cong J, Xu J, Chen K. Demonstration of etched cladding fiber Bragg grating-based sensors with hydrogel coating. Sens Actuators, B 2003;96:468–72.
[5] Sun MY, Jiang HT, Shi B, Zhou GY, Inyang HI, Feng CX. Development of FBG salinity sensor coated with lamellar polyimide and experimental study on salinity measurement of gravel aquifer. Measurement 2019;140:526–37.
[6] Gentleman DJ, Booksh KS. Determining salinity using a multimode fiber optic surface plasmon resonance dip-probe. Talanta 2006;68:504–15.
[7] Liu C, Yang L, Lu X, Liu Q, Wang F, Lv J, et al. Mid-infrared surface plasmon resonance sensor based on photonic crystal fibers. Opt Express 2017;25:14227–37.
[8] Liu C, Yang L, Liu Q, Wang F, Sun Z, Sun T, et al. Analysis of a surface plasmon resonance probe based on photonic crystal fibers for low refractive index detection. Plasmonics 2018;13:779–84.
[9] Liao Y, Wang J, Yang H, Wang X, Wang S. Salinity sensing based on microfiber knot resonator. Sens Actuators, A 2015;233:22–5.
[10] Olyaee S, Seifouri M, Karami R, Mohebzadeh-Bahabady A. Designing a high sensitivity hexagonal nano-cavity photonic crystal resonator for the purpose of seawater salinity sensing. Opt Quant Electron 2019;51:97.
[11] Guzman-Sepulveda JR, Arredondo-Lucio JA, Margulis W, May-Arrioja DA. Salinity sensor using a two-core optical fiber. Front Optics 2012:FM4H.
[12] Guzman-Sepulveda JR, Ruiz-Perez VI, Torres-Cisneros M, Sanchez-Mondragon JJ, May-Arrioja DA. Fiber optic sensor for high-sensitivity salinity measurement. IEEE Photonics Technol Lett 2013;25:2323–6.
[13] Kamil YM, Bakar MA, Syahir A, Mahdi M. Determining salinity using a singlemode tapered optical fiber. IEEE 5th international conference on photonics (ICP). 2014. p. 223–6.
[14] Stupar DZ, Bajić JS, Joža AV, Dakić BM, Slankamenac MP, Živanov MB, et al. Remote monitoring of water salinity by using side-polished fiber-optic U-shaped sensor. 15th international power electronics and motion control conference (EPE/PEMC). 2012. pp. LS4c. 4-1-LS4c. 4-5.
[15] Possetti G, Kamikawachi R, Prevedello C, Muller M, Fabris J. Salinity measurement in water environment with a long period grating based interferometer. Meas Sci Technol 2009;20:034003.
[16] Amiri IS, Paul BK, Ahmed K, Aly AH, Zakaria R, Yupapin P, et al. Tri-core photonic crystal fiber based refractive index dual sensor for salinity and temperature detection. Microwave Opt Technol Lett 2019;61:847–52.
[17] Nallusamy N, Raja RVJ, Arzate N, Torres-Gómez I. Simultaneous measurement of salinity and temperature in gold-coated D-shaped photonic crystal fiber using four-wave mixing technique. IEEE Sens Lett 2018;2:1–4.
[18] Flores R, Janeiro R, Viegas J. Optical fibre Fabry-Pérot interferometer based on inline microcavities for salinity and temperature sensing. Sci Rep 2019;9:9556.
[19] Wang S, Yang H, Liao Y, Wang X, Wang J. High-sensitivity salinity and temperature sensing in seawater based on a microfiber directional coupler. IEEE Photonics J 2016;8:1–9.
[20] Wu QL, Zhao Y, Si-Yu E, Zhang Y-N. Reflex optical fiber probe for simultaneous determination of seawater salinity and temperature by surface plasmon resonance. Instrum Sci Technol 2019;47:374–88.
[21] Zhao Y, . Ql, Wu, Zhang YN. Theoretical analysis of high-sensitive seawater temperature and salinity measurement based on C-type micro-structured fiber. Sens Actuators, B 2018;258:822–8.
[22] Wang G, Lu Y, Yang X, Duan L, Yao J. Square-lattice alcohol-filled photonic crystal fiber temperature sensor based on a Sagnac interferometer. Appl Opt 2019;58:2132–6.
[23] Kaczmarek C, Wójcik W. Measurement of pressure sensitivity of modal birefringence of birefringent optical fibers using a Sagnac interferometer. Optica Appl 2015;45.
[24] Zhao Y, Wu D, Lv RQ, Li J. Magnetic field measurement based on the Sagnac interferometer with a ferrofluid-filled high-birefringence photonic crystal fiber. IEEE Trans Instrum Meas 2016;65:1503–7.
[25] An G, Li S, An Y, Wang H, Zhang X. Glucose sensor realized with photonic crystal fiber-based Sagnac interferometer. Opt Commun 2017;405:143–6.

[26] Liu Q, Li S-G, Wang X. Sensing characteristics of a MF-filled photonic crystal fiber Sagnac interferometer for magnetic field detecting. Sens Actuators, B 2017;242:949–55.
[27] Nielsen K, Noordegraaf D, Sørensen T, Bjarklev A, Hansen TP. Selective filling of photonic crystal fibres. J Opt A: Pure Appl Opt 2005;7:L13.
[28] Wang F, Yuan W, Hansen O, Bang O. Selective filling of photonic crystal fibers using focused ion beam milled microchannels. Opt Express 2011;19:17585–90.
[29] Wang Y, Liao C, Wang D. Femtosecond laser-assisted selective infiltration of microstructured optical fibers. Opt Express 2010;18:18056–60.
[30] Cen C, Zhang Y, Chen X, Yang H, Yi Z, Yao W, et al. A dual-band metamaterial absorber for graphene surface plasmon resonance at terahertz frequency. Physica E 2020;117:113840.
[31] Cen C, Chen Z, Xu D, Jiang L, Chen X, Yi Z, et al. High quality factor, high sensitivity metamaterial graphene—perfect absorber based on critical coupling theory and impedance matching. Nanomaterials 2020;10:95.